SCAT

SCIENTIFIC COMPUTING ADVANCED TRAINING

SELF-SIMILAR AND TRAVELLING WAVE SOLUTIONS IN SURFACE TENSION-DRIVEN THIN PLANAR FILMS

by

Leonardo J. GORDILLO ZAVALETA

Contents

Acknowledgements

It is a pleasure to thank both supervisors, Christophe Josserand and Stéphane Zaleski for their comments, remarks and suggestions during the research. The author is specially thankful for their hospitality during his fellowship at the Institut Jean Le Rond D'Alembert (Laboratoire de Modélisation en Mécanique).

I acknowledge also the comments and remarks of the people who assisted to the meetings of the drop formation and bubbles group as Robert Schroll and Wendy Zhang from the University of Chicago, and Edward Spiegel from Columbia University. Special thanks to Anne Bague who helped whenever I needed, Stéphane Popinet from the NIWA[1] for the help with *Gerris* code and Laurent Duchemin from the IRPHE[2] with whom I discussed during his visit to Paris.

The whole nine-months fellowship in Paris was supported by the SCAT[3] project which is co-financed by the ALFA[4] Program of EuropAid Cooperation Office, and supported in part by the Université Pierre et Marie Curie. I am specially thankful to Boris Drappier, SCAT's Project Manager who helped me during the grant. Both supervisors and Sergio Rica from the Universidad de Chile make their best effort to get this economical support.

---

[1]National Institute of Water and Atmospheric research, New Zealand
[2]Institut de Recherche sur les Phénomènes Hors Équilibre
[3]Scientific Computing Advanced Training
[4]América Latina - Formación Académica

Introduction

My supervisors at the LMM[5] and I discussed at the beginning of the fellowship about the advantages of assisting to some courses that were going to be given by the department during the fist four months. The experience would be quite useful for the second stage of the fellowship: the five-months research. I assisted to several courses including: *Introduction to hydrodynamics instabilities*, *Multi-scale phenomena in hydrodynamics*, *Introduction to numerical methods in fluid mechanics*, *Multi-phase flows: drop and bubbles dynamics*, *Compressible flows instabilities*, *Suspensions and diphasic flows*, *Vortex in hydrodynamics*, *Open flow instabilities* and *Control flow*. The courses were dictated at the University Campus at Jussieu and some of them at the École Polytechnique at Lozère.

This report is focused on the research of the second part of the fellowship. I joined the drops and bubbles group led by Stéphane Zaleski. The group meetings with the Department members and other foreign visitors were quite useful in the development of this work. Every week, I had to show the advances of my research where my procedures and results were discussed.

The generation of drops has been a topic of great interest since a long time ago between physicists. The process is fascinating complicate. The first successful explanation of the physics that produces the breakup of a free surface flow into drops was done by Laplace in 1805 when he identified the surface tension as the responsible of the instability that carries out the process. In 1879, Rayleigh noticed that surface tension should work against inertia. By a simple linear stability analysis, he found that a fluid cylinder was unstable to small perturbations of its shape finding an optimal perturbation wavelength of about nine times the radius of the cylinder. The cylinder then should break up into drops of a typical size given by this wavelength. His results were confirmed by him with great success.

However, Rayleigh's theory was not able to predict other related phenomena such as satellite drops in breakups. A hundred years passed until the nonlinear

---

[5]Laboratoire de Modélisation en Mécanique

Figure 1: Water splash crown. A thick rim is formed at the edge of the crown and fingers of fluid are ejected from it. From the fingers, drops are ejected to the surrounding air. *Public access photograph at Flickr*$^{\mathrm{TM}}$

theories boost gave to the problem new tools for understanding the process near the breakup. The first attempt was done by the *lubrication theory* or *shallow-water approximation*. Using this equations, Eggers and Dupont in 1994[2] showed that an axisymmetrical jet may contract radially reaching zero in finite time without considering any microscopic process.

The goal of our research was to investigate the nature of the process which occurs in a two-dimensional liquid viscous sheet that retracts by the action of surface tension. Until now, the research has mainly consisted in numerical simulations and here we have tried to develop some analytical tools to give asymptotic behavior of the solutions. Curiously, the whole problem is controlled by just one parameter consisting in the rate between viscous and surface tension forces and it should be linked directly to the eventual breakup criterion. Understanding well this subject could help to solve a lot of more complicated phenomena as the splash crown where a cylindrical sheet is ejected upward. A *fingering* process takes place there. From the tips of this fingers, drops can be ejected following the axisymmetrical pinch-off. Other phenomena, such as growing holes in sheets which are very important in the industry of curtain coating, may be also better understood.

The plan of the work is the following: Chapter I gives a brief theoretical introduction to the topic. The second one consists in the main analysis of the research, the study of the lubrication equations when describing retracting sheets. The third one is addressed to some numerical simulations we have done and the results discussion.

Chapter 1

Dynamics of free surface 2-D fluid sheets

In this chapter we give a brief overview of the dynamics of thin two-dimensional fluid sheets bounded by free surfaces. These sheets may have a free edge. We consider first the theoretical results for the speed at which the edge moves. Then we will study the motion of unbounded 2-D sheets by linear analysis, paying special attention to varicose modes. Finally, we will review the expansion of Navier-Stokes equations for long wavelength perturbations that leads to lubrication equations.

1.1   The Taylor-Culick velocity

Thin sheets of fluid that have a free edge retract because of surface tension. When they retract, their edges grow as they collect mass from the sheet forming a thick rim. Using very simple arguments, Taylor and Culick in 1959[9] found independently that the velocity at which the edge of a 2-D fluid sheet moves into it is constant.

The rim retracts at a constant speed,

$$c_{\text{rim}} = \sqrt{\frac{\sigma}{\rho e}}, \tag{1.1}$$

and the result is absolutely independent of viscosity. However, viscosity should play a role in some manner. This would be discussed further.
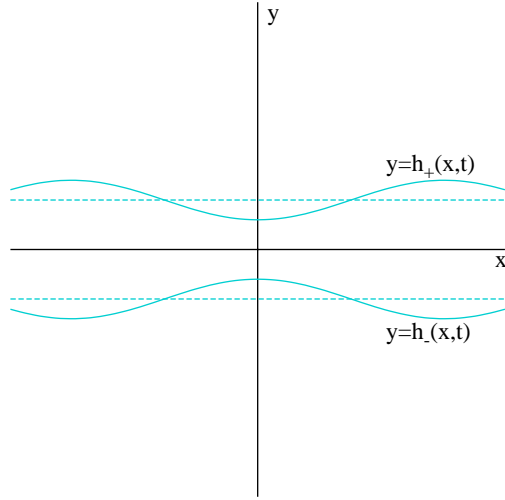
Figure 1.1: Thin 2-D fluid sheet scheme: the interfaces $h_+(x,t)$ and $h_-(x,t)$ are considered as free surfaces. The length scale of the problem is e, the mean value of the width of the 2-D fluid sheet , shown as a dashed line.

1.2 Navier-Stokes equations for a 2-D fluid sheet

We consider a viscous liquid two-dimensional fluid sheet immersed in a gas with a density low enough to consider the boundaries as free surfaces. The 2-D fluid sheet is thick enough as well to apply continuum mechanics. The problem is governed by the 2-D Navier-Stokes and the incompressibility equations.

The system of equations can be rescaled in the following way: the lengths as $x, y, h \sim e$; the time as $t \sim e^2/\nu$; the velocities as $u, v \sim \nu/e$ and finally the pressure as $P \sim \rho\nu^2/e^2$. We have defined $2e$ as the mean thickness of the 2-D fluid sheet. The rescaling drops all the physical parameter leaving a non-dimensional system. The whole system is controlled by just one dimensionless parameter Z defined as,

$$Z^2 = \frac{\rho\nu^2}{\sigma e}, \tag{1.2}$$

known as Ohnesorge's number. This parameter represents the ratio between the viscous and surface tension forces in a characteristic length of the 2-D fluid sheet.

Our final non-dimensional set of nonlinear partial differential equations is given by,

$$\partial_t u + u\partial_x u + v\partial_y u = -\partial_x p + (\partial_{xx} u + \partial_{yy} u), \tag{1.3a}$$

$$\partial_t v + u\partial_x v + v\partial_y v = -\partial_y p + (\partial_{xx} v + \partial_{yy} v), \tag{1.3b}$$

$$\partial_x u + \partial_y v = 0. \tag{1.3c}$$

and the three of the following boundary conditions at $y = h(x, t)$ and the fourth at $y = 0$,

$$v = \partial_t h + u \partial_x h, \tag{1.4a}$$

$$\partial_y u + \partial_x v = 2 \frac{\partial_x h (\partial_y v - \partial_x u)}{(1 + \partial_x h^2)}, \tag{1.4b}$$

$$-p + 2 \frac{(1 - \partial_x h^2) \partial_y v - \partial_x h (\partial_y u + \partial_x v)}{1 + \partial_x h^2} = Z^{-2} \frac{\partial_{xx} h}{(1 + \partial_x h^2)^{\frac{3}{2}}}, \tag{1.4c}$$

$$\partial_y u = v = 0. \tag{1.4d}$$

where we have added symmetry across the y-axis. We have not considered in the previous equations microscopic forces like those studied by Van der Waals.

1.2.1 Waves in uniform sheets

How does the system react when small perturbations are applied? It is well known that capillarity waves appear. On the other hand, the effect of viscosity is just to dissipate energy. We found the exact solution and the properties of this waves in the case of varicose modes. Our calculation is similar to Lamb's 1932[4] calculation for shallow water waves.

For this purpose, we study the perturbations of an unbounded sheet at rest of thickness $2e$. This can be written in the non-dimensional variables as,

$$u(x, y, t) = \epsilon u_1(x, y, t),$$
$$v(x, y, t) = \epsilon v_1(x, y, t),$$
$$p(x, y, t) = \epsilon p_1(x, y, t),$$
$$h(x, t) = 1 + \epsilon h_1(x, t).$$

It is quite useful to rewrite the system in terms of the velocity potential $\varphi(x, y, t)$ and the stream function $\psi(x, y, t)$,

$$u_1 = -\partial_x \varphi_1 - \partial_y \psi_1, \tag{1.5a}$$

$$v_1 = -\partial_y \varphi_1 + \partial_x \psi_1. \tag{1.5b}$$

The solutions of the resulting system of equations are now given by,

$$\varphi_1(x, y, t) = (Ae^{ky} + Be^{-ky})e^{ikx+st},$$

$$\psi_1(x, y, t) = (Ce^{qy} + De^{-qy})e^{ikx+st},$$

where $q^2 - k^2 = s$ from the Navier-Stokes equations. Here the y-symmetry eliminates quickly the number of constants to two and $\cosh$ and $\sinh$ appear naturally in the solution. Replacing this expressions in the other three boundary conditions

should gives us the dispersion relation of varicose modes over the sheet. This is equivalent to impose the determinant equal to zero,

$$
\begin{vmatrix}
-k & ik & -s \\
2ik^2 & 2k^2 + s & 0 \\
-(2k^2 + s)\coth k & 2iqk\coth q & Z^{-2}k^2
\end{vmatrix} = 0.
$$

The dispersion relation has an interesting limit for long-wave perturbations, or equivalently $k \to 0$. Using that $\lim_{x \to 0^+} \coth x = x^{-1}$, we can write,

$$
Z^{-2}k^4 + (2k^2 + s_{\mathrm{lw}})^2 = 4k^4
$$

and this equation has two roots,

$$
s_{\mathrm{lw}}(k) = -2k^2 \left(1 \pm \sqrt{1 - \frac{1}{4Z^2}} \right).
$$

The real part of $s(k)$ will always be negative. However, the existence of an imaginary part depends on the Ohnesorge's number. If $Z \geq \frac{1}{2}$, the two roots are negative and real while for $Z < \frac{1}{2}$, the two roots are complex with a negative real part as well. When Z is very small, we can obtain the limit of inviscid capillary waves,

$$
s_{\mathrm{lw}}(k) = -2k^2 \left(1 \pm i\frac{1}{2Z} \right).
$$

Therefore, the velocity at which the long waves propagate is independent of the viscosity,

$$
c_{\mathrm{lw}} = \sqrt{\frac{\sigma e}{\rho}}\, k \tag{1.6}
$$

There is an other interesting limit for short waves. In this case, $k \to 0$ and now we can use $\lim_{x \to \infty^+} \coth x = 1$. Using that $s \sim k$, we find the following expression to the first order,

$$
Z^{-2}k^4 + (2k^2 + s_{\mathrm{sw}})^2 = 4k^4 \left(1 + \frac{s_{\mathrm{sw}}}{2k^2} \right),
$$

and s_{sw} can be easily found,

$$
s_{\mathrm{sw}}(k) = -\frac{k}{2Z^2}.
$$

This shows that all short waves are damped and the rate at which this occurs depends inversely on the Ohnesorge number. Moreover, no travelling waves exist in this limit as the root is strictly real.

We can confirm that for any Ohnesorge number, all the oscillations are damped, those of smaller wavelength in a more effective way. As the Ohnesorge number grows, the oscillations need more time to be damped as viscosity decelerates the process. In the long wave an small Ohnesorge's number limit, the waves are very-weakly damped while in the short wave limit, they are damped with a rate inversely proportional to the Ohnesorge number.

1.3   The long-wave theory

Erneux and Davis found in 1993[3] a set of coupled equations for long-wave perturbations in 2-D fluid sheets. They started from the Navier-Stokes equations and the free-surface boundary conditions at the interfaces. They made an asymptotic expansion of the system using the wave-number as small parameter obtaining as result a set of two coupled nonlinear equations that involve the thickness of the fluid sheet and its horizontal velocity. The set of equations have been commonly used when studying this kind of fluid sheets, *e. g.* linear stability theory, Erneux and Davis 1993[3].

   The long-wave theory consists in expanding equations (1.3) and (1.4) using the following scalings,

$$
\begin{array}{lll}
\xi = kx, & \psi = y, & \tau = k^2 t \\
U = k^{-1}u, & V = k^{-2}v, & P = k^{-2}p \\
H = h, & \overline{Z} = Z
\end{array}
\tag{1.7}
$$

where k is defined as a dimensionless wave-number and will be used as the small parameter. The system admits an expansion in terms of this parameter of the following form,

$$
(U, V, P) = (U_0, V_0, P_0) + k^2 (U_1, V_1, P_1) + ...
\tag{1.8}
$$

Replacing this expansion in our set of equations leads to a sequence of problems after equating similar powers of k. The two first orders give us the following set of equations known as lubrication equations,

$$
\partial_t h + \partial_x(hu) = 0
\tag{1.9a}
$$

$$
h\partial_t u + hu\partial_x u = 4\partial_x(h\partial_x u) + Z^{-2}h\partial_{xxx}h
\tag{1.9b}
$$

or in the physical variables,

$$
\partial_t h + \partial_x(hu) = 0,
\tag{1.10a}
$$

$$
h\partial_t u + hu\partial_x u = 4\nu\partial_x(h\partial_x u) + \frac{\sigma}{\rho}h\partial_{xxx}h,
\tag{1.10b}
$$

It is remarkable than the viscous term includes an extra coefficient $4h$ with respect to usual Navier-Stokes equations called *Trouton* viscosity. The factor 4 is fairly the ratio of the elongational to the shear viscosity for viscous flows.

Chapter 2

Asymptotic solution for a retracting 2-D fluid sheet

In this chapter, we try to look for solutions of the problem of a fluid sheet that retracts by the action of surface tension. To achieve this, we use the lubrication equations introduced in Chapter 2 that may describe in a simpler way the dynamics of the fluid sheet.

2.1 Asymptotic travelling wave solutions far from the rim

The goal of the analysis was to look for solutions of the lubrication equations that travel with constant speed. The long-wave limit lubrication equations were found by Erneux and Davis 1993[3]. The equations used here include the complete curvature term as Brenner and Gueyffier 1990[1] introduced it following successful numerical results obtained by Eggers and Dupont 1994[2] for axisymmetrical jets. These solutions may represent the behavior far from the edge as time goes to infinity.

2.1.1 Leading order travelling waves solutions

The set of equations that describes the thickness and the horizontal velocity of the fluid sheet was found in Chapter 1,

$$\partial_t h + \partial_x(hu) = 0, \tag{2.1a}$$

$$h\partial_t u + hu\partial_x u = 4\nu\partial_x(h\partial_x u) + \frac{\sigma}{\rho}h\partial_x\left(\frac{\partial_{xx}h}{\sqrt{1 + \partial_x h^2}^3}\right), \tag{2.1b}$$

but now we have included the curvature correction as Brenner and Gueyffier did it in 1990[1]. The two boundary conditions, $h = e$ and $u = 0$ at $x \to \infty$. We look

9

for solutions that translates with velocity c as,

$$\begin{cases} h(x,t) &= h_{\text{tw}}(z,\tau), & z &= x - ct, \\ u(x,t) &= u_{\text{tw}}(z,\tau), & \tau &= t. \end{cases} \tag{2.2}$$

Navier-Stokes equations and lubrication equations are invariant under Galilean transformations, so from here, we will place ourselves in an inertial frame of reference travelling at speed c. The equations then are the same but with the new boundary conditions $h = e$ and $u = -c$ at $z \to \infty$. We will try to make an asymptotic expansion of the solution of this equation when $t \to \infty$ of the form,

$$h_{\text{tw}}(z,\tau) = \sum_{n=0}^{\infty} \tau^{-n} h_{\text{tw}_n}(z), \qquad u_{\text{tw}}(z,\tau) = \sum_{n=0}^{\infty} \tau^{-n} u_{\text{tw}_n}(z). \tag{2.3}$$

The leading order when replacing expresions (2.15) in equations (2.1) leads us to one single nonlinear equation given by,

$$c^2 e^2 \left(\frac{1}{h_{\text{tw}_0}} - \frac{1}{e} \right) = 4\nu c e \left(\frac{\partial_z h_{\text{tw}_0}}{h_{\text{tw}_0}} \right) + \frac{\sigma}{\rho} \left(\frac{1 + \partial_z h_{\text{tw}_0}^2 + h_{\text{tw}_0} \partial_{zz} h_{\text{tw}_0}}{\sqrt{1 + \partial_z h_{\text{tw}_0}^2}^3} \right) - \frac{\sigma}{\rho}. \tag{2.4}$$

In this equation, there are two terms that may be cancelled for a given value of the velocity c. These two terms which do not depend on $h_{\text{tw}_0}(z)$ —the second term in the left hand side and the last term in the right hand side— represent respectively the flux of momentum into the fluid and the surface tension pull force both at infinity. If we balance these two terms, we find a value for c,

$$c = \sqrt{\frac{\sigma}{e\rho}}, \tag{2.5}$$

which is the result of Taylor 1959[9] and Culick 1960 for the velocity at which a fluid sheet retracts using momentum conservation arguments. Replacing this result in the equation and after making it dimensionless by the following rules $h \sim e$, $z \sim e$ and considering the dimensionless parameter defined in (1.2), we obtain the following second ordinary differential equation which just depends on the Ohnesorge number:

$$-\frac{1 - 4Z\partial_z h_{\text{tw}_0}}{h_{\text{tw}_0}} + \frac{1 + \partial_z h_{\text{tw}_0}^2 + h_{\text{tw}_0} \partial_{zz} h_{\text{tw}_0}}{\sqrt{1 + \partial_z h_{\text{tw}_0}^2}^3} = 0, \tag{2.6}$$

with the boundary condition $h_{\text{tw}_0}(\infty) \to 1$ and $\partial_z h_{\text{tw}_0}(\infty) \to 0$.

2.1.2 The $z \to \infty$ limit

Equation (2.6) has an attractor at $h_{\mathrm{tw}_0} = 1$ as z approaches ∞. It would be useful to look for perturbations near the stable point $h_{\mathrm{tw}_0} = 1$. Replacing $h_{\mathrm{tw}_0}(z) = 1 + \epsilon \tilde{h}_{\mathrm{tw}_0}(z)$ leads us to the following linear equation:

$$\partial_{zz}\tilde{h}_{\mathrm{tw}_0} + 4Z\partial_z\tilde{h}_{\mathrm{tw}_0} + \tilde{h}_{\mathrm{tw}_0} = 0. \tag{2.7}$$

We try solutions of the form $\tilde{h}_{\mathrm{tw}_0}(z) = e^{qz}$. This can let us find the characteristic shape of the solutions where the typical scale of length is now given by,

$$q = -2Z \pm \sqrt{4Z^2 - 1}. \tag{2.8}$$

From here, we can see that for $Z > Z_c = \frac{1}{2}$, the solutions decay monotonically while for $Z < Z_c$ the solutions oscillate while they decay.

In the large Ohnesorge number limit, we obtain two scales, a very fast one: $q = -4Z$ and a slow one $q = -(4Z)^{-1}$ as the exact limit solution found by Sünderhauf, Raszillier and Durst 2002[8]. On the other hand, in the limit of small Ohnesorge's number, we obtain $q = -2Z \pm i$. Here the wavelength oscillation does not depend anymore on the Ohnesorge number. The parameter just controls the scale of the exponential envelope of the oscillations. The wavelengths of the oscillations in this case $\lambda = 2\pi e$ seem to be in agreement with the complete Navier-Stokes Simulations performed by Song and Tryggvason 1998[7].

2.1.3 The flow phase field plot and whole domain solutions

The equation that we have obtained is autonomous so a flow phase field plot (see Fig. 2.1) may help us to study the behavior of its solutions. Autonomous ordinary differential equations are also invariant under translations. If $h_{\mathrm{tw}_0}(z)$ is solution of the equation then $h_{\mathrm{tw}_0}(z - z_0) \ \forall z_0$ is also solution.

The field plot near the stable point $(h_{\mathrm{tw}_0}, \partial_z h_{\mathrm{tw}_0}) = (1, 0)$ shows that there is a well defined trajectory around it. Zooming out, the field plots shows the solutions may come from $\partial_z h_{\mathrm{tw}_0} = \pm\infty$. Moreover, they show that these derivative divergencies occur for z finite. However, there is a parabolic-like solution that acts as a separatrix between these behaviors which is well defined for all z.

The asymptotic behavior of the derivative-divergent solutions is obtained by the following balance in the equation as $h_{\mathrm{tw}_0} \to C_0$ and $\partial_z h_{\mathrm{tw}_0} \to \pm\infty$, that leads to a solution,

$$h_{\mathrm{tw}_0}(z) \sim C_0 \pm \left(\frac{9C_0^2}{32Z}\right)^{\frac{1}{3}} (z - z_0)^{\frac{2}{3}}. \tag{2.9}$$

On the other hand, another balance is possible when $\partial_z h_{\mathrm{tw}_0} \gg (4Z)^{-1}$, leading to

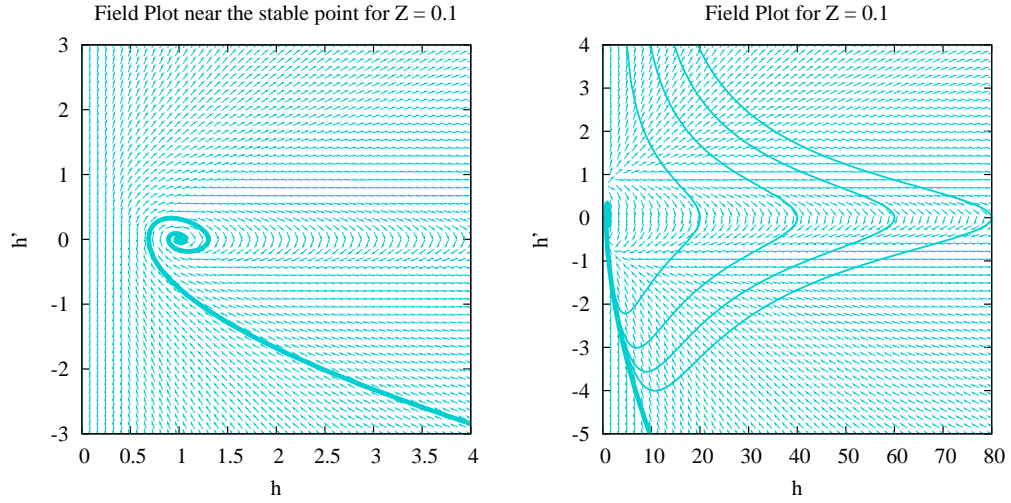$$-h_{\mathrm{tw}_0}\partial_z h_{\mathrm{tw}_0}\sqrt{C_1 + \frac{8}{3}Zh_{\mathrm{tw}_0}^{-3}} = 1.$$

Figure 2.1: Field plots showing the behavior near the stable point and at a large scale for Z = 0.1. Only some of the solutions whose derivatives go to $\partial_z h_{\mathrm{tw}_0} \rightarrow +\infty$ as $z \rightarrow -\infty$ are shown. We can notice the formation of the envelope when we approach the stable point.

The behavior of the solution can be divided in two parts. An inner core when $h_{\mathrm{tw}_0} \ll \sqrt[3]{8Z/3C_1}$. This is led by the left branch of the parabola,

$$h_{\mathrm{tw}_0}(z) \sim \frac{3}{32Z}(z - z_0)^2. \tag{2.10}$$

This fist solution is the separatrix on the plane z—h_{tw_0} between the derivative-divergent solutions. In the physical space, it appears as an envelope between these two kinds of solutions as it is shown in Fig. 2.2. The derivative-divergent solutions have been appropriately translated to fit in the envelope.

This envelope solution develops a tail in the positive direction as $z \rightarrow \infty$ whose shape remains invariant by changing the boundary condition. Its shape is merely determined as it has seen before in section 2.1.2 by the parameter Z.

On the other hand, the outer core does depend in the constant of integration C_1. In the region $h_{\mathrm{tw}_0} \gg \sqrt[3]{8Z/3C_1}$, is led by,

$$h_{\mathrm{tw}_0}(z) \sim \left(\frac{4}{C_1}\right)^{\frac{1}{4}} \sqrt{z_0 - z}, \tag{2.11}$$

and gives us the asymptotic shape of the function when returning to $\partial_z h_{\mathrm{tw}_0} = 0$. This can be seen in Fig. 2.1 where they appear as a zone where the function resembles the curve $\partial_z h_{\mathrm{tw}_0} \sim -1/h_{\mathrm{tw}_0}$. This zone seem to be very important when performing the matching with the self-similar part.
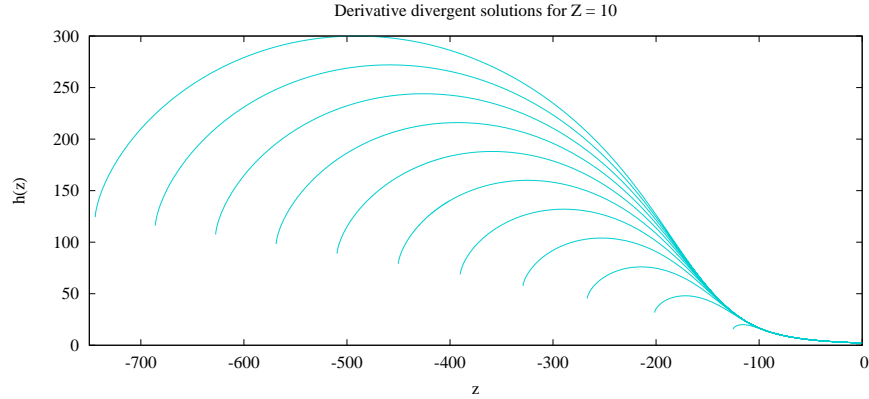
Figure 2.2: Set of solutions showing the shape of the envelope with different boundary conditions s at $Z = 10$. The left side of the solutions show the appearance of the derivative singularity.

There is another interesting limit of equations when $h_{\mathrm{tw}_0} \gg 1$, which gives us,

$$h_{\mathrm{tw}_0}(z) \sim \sqrt{C^2 - (z - z_0)^2}, \tag{2.12}$$

which corresponds to a circle and is independent of the Ohnesorge number. This solution is the continuation of the function found at (2.11) and the again the constants do not affect the solution when $z \to \infty$.

2.2 Asymptotic self-similar solutions for the growing rim

After studying the travelling wave solutions that could describe the shape of the fluid sheet far from the rim, we proceed to study solutions that show self-similar behavior as those found by numerical simulations of the complete Navier-Stokes equations (Song and Tryggvason 1998[7]).

Both complete Navier-Stokes equations and lubrication equations show that there exists solutions that become self-similar as $t \to \infty$. This appears as a slow time dependence in the equations after replacing the self-similar variables. In both cases, this is achieved by:

$$\begin{cases} h(x,t) & = & t^{\frac{1}{2}} & h_{\mathrm{ss}}(\xi,\tau), & \xi & = & xt^{-\frac{1}{2}}, \\ u(x,t) & = & t^{-\frac{1}{2}} & u_{\mathrm{ss}}(\xi,\tau), & \tau & = & t, \end{cases} \tag{2.13}$$

where the following rescalings have already been made: $x \sim e$, $h \sim e$, $t \sim \frac{e}{c}$ and $u \sim c$.

2.2.1 Leading order self-similar solutions

The set of transformations (2.13) applied to lubrication equations (2.1), leads us to the following set of coupled equations,

$$
\begin{cases}
\tau \partial_\tau h_{\text{ss}} + \frac{1}{2} h_{\text{ss}} - \frac{1}{2} \xi \partial_\xi h_{\text{ss}} + \partial_\xi (h_{\text{ss}} u_{\text{ss}}) & = & 0 \\
\tau \partial_\tau u_{\text{ss}} - \frac{1}{2} u_{\text{ss}} - \frac{1}{2} \xi \partial_\xi u_{\text{ss}} + u_{\text{ss}} \partial_\xi u_{\text{ss}} - \frac{4Z}{h_{\text{ss}}} \partial_\xi (h_{\text{ss}} \partial_\xi u_{\text{ss}}) & = & \tau^{\frac{1}{2}} \partial_\xi \left(\frac{\partial_{\xi\xi} h_{\text{ss}}}{\sqrt{1 + \partial_\xi h_{\text{ss}}^2}^3} \right)
\end{cases} .
$$
(2.14)

The solution of this equations may admit a series expansion when $t \to \infty$ in powers of $t^{-\frac{1}{2}}$,

$$
h_{\text{ss}}(\xi, \tau) = \sum_{n=0}^{\infty} \tau^{-\frac{n}{2}} h_{\text{ss}_{n/2}}(\xi), \qquad u_{\text{ss}}(\xi, \tau) = \sum_{n=0}^{\infty} \tau^{-\frac{n}{2}} u_{\text{ss}_{n/2}}(\xi).
$$
(2.15)

When replacing this, we obtain a set of ordinary differential equations for the leading order and subsequent linear sets for higher orders. The leading order set of equations is invariant under the two following transformations $h_{\text{ss}_0} \to R h_{\text{ss}_0}$, $u_{\text{ss}_0} \to u_{\text{ss}_0}$, $\xi \to \xi/R$, and $\xi \to \xi - \xi_0$, $u_{\text{ss}_0} \to u_{\text{ss}_0} + \xi_0/2$. The solutions are given by,

$$
h_{\text{ss}_0}(\xi) = \sqrt{1 - \xi^2}
$$
(2.16a)

$$
u_{\text{ss}_0}(\xi) = -\frac{1}{4} \left(\frac{\pi + 2 \arcsin \xi}{\sqrt{1 - \xi^2}} \right)
$$
(2.16b)

Turning back to the physical variables, we have obtained the leading order expansion for the growing rim,

$$
h_{\text{ss}_0}(z) = \sqrt{R^2 t - \left(z - \sqrt{t} z_0^* \right)^2}
$$
(2.17)

The value of R can be found by conservation of mass principle. The growing rim must support the flux of fluid coming from infinity, so we have,

$$
R = \sqrt{\frac{2}{\pi}}.
$$
(2.18)

2.3 The intermediate matching region

We have already found leading order expressions for the unperturbed region and the growing rim of the fluid sheet. In the first case, we had found that there was a parabolic envelope near the solution that could support any function coming from $h_{\text{tw}_0} \to \infty$. In the second case we have found circular solutions, whose

asymptotic behavior corresponds to a square root as we approach $h_{\mathrm{ss}_0} \to 0$. Then, the matching region should satisfy the following limits,

$$
h_{\mathrm{m}}(h \to 1) \quad \sim \quad \frac{3}{32\mathrm{Z}}(z - z_0)^2, \tag{2.19a}
$$

$$
h_{\mathrm{m}}(h \to \infty) \quad \sim \quad t^{\frac{1}{4}} \sqrt{-2R(z - (z_0^* + R)t^{\frac{1}{2}})}. \tag{2.19b}
$$

There must exist a new intermediate scaling of variables, between those we have already found, whose leading order satisfies this limits. The scaling would be attained when doing the proper balance in lubrication equations. In fact, we have already found in section 2.1.3 that the balance is given between the surface tension and the viscosity terms. The scaling that achieves this, is given by,

$$
\begin{cases}
h(x,t) &= t^{\frac{1}{3}} \quad h_{\mathrm{m}}(\zeta, \tau), \qquad \zeta = xt^{-\frac{1}{6}}, \\
u(x,t) &= t^{-\frac{1}{3}} \quad u_{\mathrm{m}}(\zeta, \tau), \qquad \tau = t,
\end{cases} \tag{2.20}
$$

Replacing this new scalings in the lubrication equations leads us to,

$$
\begin{cases}
\tau^{\frac{1}{6}}\partial_\tau h_{\mathrm{m}} + \tau^{-\frac{1}{2}}\left(\frac{1}{3}h_{\mathrm{m}} - \frac{1}{6}\zeta\partial_\zeta h_{\mathrm{m}}\right) + \partial_\zeta(h_{\mathrm{m}}u_{\mathrm{m}}) &= 0, \\
\\
\tau^{\frac{2}{3}}\partial_\tau u_{\mathrm{m}} - \tau^{-\frac{2}{3}}\left(\frac{1}{3}u_{\mathrm{m}} + \frac{1}{6}\zeta\partial_\zeta u_{\mathrm{m}}\right) + \tau^{-\frac{1}{6}}u_{\mathrm{m}}\partial_\zeta u_{\mathrm{m}} &= \frac{4\mathrm{Z}}{h_{\mathrm{m}}}\partial_\zeta(h_{\mathrm{m}}\partial_\zeta u_{\mathrm{ss}}) + .. \\
& \qquad \tau^{\frac{1}{2}}\partial_\zeta\left(\frac{\partial_{\zeta\zeta}h_{\mathrm{m}}}{\sqrt{1+\tau^{\frac{1}{3}}\partial_\zeta h_{\mathrm{m}}^2}^3}\right).
\end{cases} \tag{2.21}
$$

Again, we will try an expansion now in powers of $t^{-\frac{1}{6}}$,

$$
h_{\mathrm{m}}(\zeta,\tau) = \sum_{n=0}^{\infty} \tau^{-\frac{n}{6}} h_{\mathrm{m}_{n/6}}(\zeta), \qquad u_{\mathrm{m}}(\zeta,\tau) = \sum_{n=0}^{\infty} \tau^{-\frac{n}{6}} u_{\mathrm{m}_{n/6}}(\zeta), \tag{2.22}
$$

the leading order can be simplified into the following equation

$$
-4\mathrm{Z}\left(\frac{\partial_\zeta h_{\mathrm{m}_0}}{h_{\mathrm{m}_0}}\right) = \frac{\partial_{\zeta\zeta}h_{\mathrm{m}_0} + \partial_\zeta h_{\mathrm{m}_0}^2}{\sqrt{\partial_\zeta h_{\mathrm{m}_0}^2}^3}.
$$

The properties of this equation were already studied in section 2.1.3. Its solution is given implicitly by,

$$
-\int h_{\mathrm{m}_0}\sqrt{B_1^2 + \frac{8\mathrm{Z}}{3}h_{\mathrm{m}_0}^{-3}}\,\mathrm{d}h_{\mathrm{m}_0} = \zeta - B_2. \tag{2.23}
$$

2.4 The whole domain matched solution

The constants B_1 and B_2 remain to be fixed by a matching between the other regions. In the limit $h_{\mathrm{m}_0} \to \infty$, the asymptotic expansion of equation (2.23) is,

$$
-\frac{1}{2}B_1 h_{\mathrm{m}_0}^2 - \left(\frac{24\mathrm{Z}^2}{B_1}\right)^{\frac{1}{3}}\int_0^1 \frac{\mathrm{d}s}{\sqrt{3s^4 - 3s^2 + 1}} + \mathcal{O}(h_{\mathrm{m}_0}^{-1}) = \zeta - B_2
$$

The other relevant expansion when $h_{\mathrm{m}_0} \to 0$ is given by,

$$\left(\frac{32Z}{3}\right)^{\frac{1}{2}} h_{\mathrm{m}_0}^{\frac{1}{2}} - \left(\frac{3}{392Z}\right)^{\frac{1}{2}} B_1^2 h_{\mathrm{m}_0}^{\frac{7}{2}} + \mathcal{O}(h_{\mathrm{m}_0}^{\frac{11}{2}}) = \zeta - B_2.$$

Turning back to the physical plane, for the leading orders, we have,

$$-\frac{1}{2} B_1 t^{-\frac{2}{3}} h^2 = t^{-\frac{1}{6}} z - B_2, \tag{2.24a}$$

$$\left(\frac{32Z}{3}\right)^{\frac{1}{2}} t^{-\frac{1}{6}} h^{\frac{1}{2}} = t^{-\frac{1}{6}} z - B_2. \tag{2.24b}$$

The matching will allow us to fix the constants. The last expression shows that the matching with the fluid sheet is guaranteed when $B_2 = 0$. For the outer region, we need to match (2.24a) with (2.19b). The constants are then,

$$B_1 = R^{-1}, \qquad\qquad B_2 = 0. \tag{2.25}$$

Moreover, is necessary also that $z_0^* = -R$. With this, we can construct a the leading order solution for the whole domain. We express it as an explicit combination of the travelling wave, the self-similar and the intermediate solutions,

$$h(z,t) = h_{\mathrm{tw}_0}(z-z_0) + t^{\frac{1}{3}} h_{\mathrm{m}_0}\left(\frac{z}{t^{\frac{1}{6}}}\right) + t^{\frac{1}{2}} h_{\mathrm{ss}_0}\left(\frac{z}{t^{\frac{1}{2}}}\right) - \mathrm{H}(-z)\left(\frac{3}{32Z} z^2 + t^{\frac{1}{4}} (-2Rz)^{\frac{1}{2}}\right), \tag{2.26}$$

where $\mathrm{H}(z)$ is the Heaviside function[1].

The general matching scheme is shown in Fig. 2.3. The intermediate and the travelling wave region and can be seen as double boundary layers shrinking with time when viewed from the self-similar reference frame.

Even we had found this asymptotic time-dependant whole domain solution, we do not have an analytical solution for the travelling-wave region. In order to obtain a view of the result, we need to find a method that fixes the last constant of the matching z_0. This is not an easy task and we have determined it numerically.

The strategy is to start integrating numerically the travelling wave equation *downward* from an initial condition that coincides with the asymptotic shape of the parabola centered at the origin. Even we start with this initial condition, this is not a guarantee that our constant z_0 is zero because $h \sim z^2$ is just the leading order and we may have other orders that are not convergent like $h \sim z$. Moreover, there is also a tail of zero order. After fixing this, we can adjust z_0 in such a way that the order z_1 falls to zero. To achieve this, we had calculated a difference between the original parabola and the numerical solution which should give us,

$$h_{\mathrm{tw}_0}(z) - \frac{3}{32Z} z^2 = \frac{3}{32Z}(z - z_0)^2 - \frac{3}{32Z} z^2 \sim \left(-\frac{3z_0}{16Z}\right) z.$$

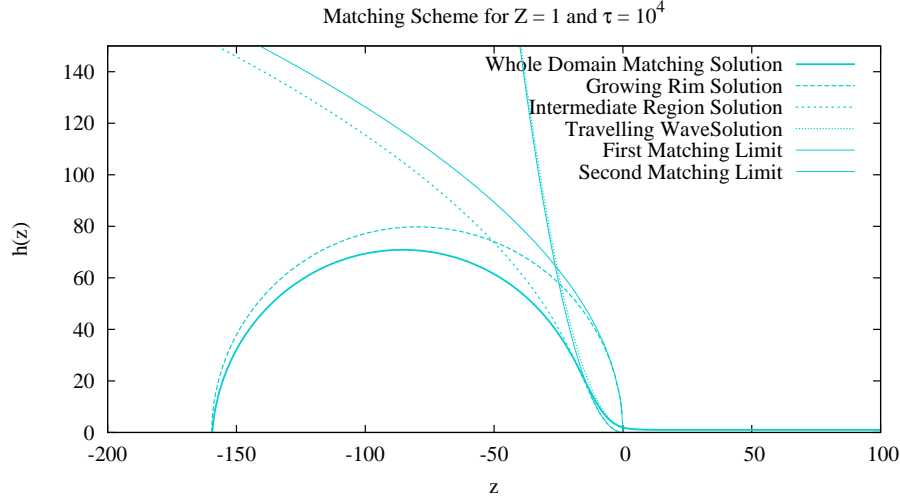[1]We have included as the matching limit shape is just the left branch of the parabola.

Figure 2.3: Matching scheme showing the different regions of the problem: the circular self-similar solution, the travelling wave solution far from the rim and the intermediate region which links them.

Then the final initial condition can be calculated finding the slope of the difference between this two curves. This was performed by a linear fit by a least-square method. However, it is necessary to look for a region where the difference between these two functions tends to a straight line.

Once z_0 has been fixed, the whole domain solution can be found as it is shown in Fig. 2.4 which show the evolution of time of the solution.

2.4.1 Convergence of the matched solutions

There are two small tails of order zero for the matching limits of the functions used when finding the whole domain solution. The matching between the growing rim and the intermediate region has a tail given by,

$$B_{\text{ss-m}} = \left(24R^{-1}Z^2\right)^{\frac{1}{3}} \int_0^1 \frac{\mathrm{d}s}{\sqrt{3s^4 - 3s^2 + 1}} t^{\frac{1}{4}} \sim Z^{\frac{2}{3}} t^{\frac{1}{4}}. \tag{2.27}$$

On the other hand, the tail associated to the matching limit of the intermediate and unperturbed region seems to be proportional to the inverse of Ohnesorge's number,

$$B_{\text{m-tw}} \sim Z^{-1}. \tag{2.28}$$

Both tails should be much smaller than the typical size of the rim $t^{\frac{1}{2}}$. This condition gives us the following convergence criteria,

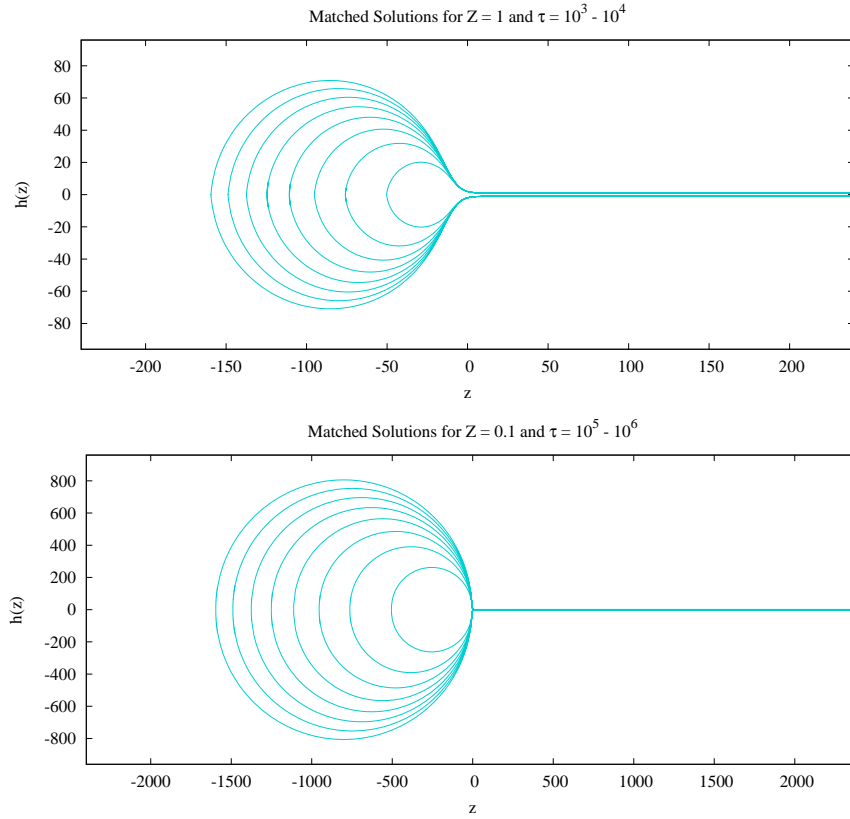$$Z^{\frac{2}{3}} t^{\frac{1}{4}}, Z^{-1} \ll t^{\frac{1}{2}}$$

Figure 2.4: Time evolution of the matched solutions at $Z = 1$ and $Z = 0.1$ between $\tau = 10^3$ to 10^4 and $\tau = 10^5$ to 10^6 respectively.

or in terms of t,

$$t \gg Z^{-2}, Z^{\frac{8}{3}}, \tag{2.29}$$

which means that this kind of solution is reached for two different time scales depending on the Ohnesorge number. For large Ohnesorge's number, this solution is valid when time is much greater than the eight thirds power of Z, while for low Ohnesorge's number, we will have to wait until the time is much greater than the inverse of the square of Z. This results seem to be qualitatively in accord with numerical simulations where larger Ohnesorge numbers played the role of delaying the convergence to the Taylor-Culick velocity. For low Ohnesorge's numbers, where the Taylor-Culick velocity is reached quickly, these criteria could be related to the existence of other regimes with different scalings. This would lead us to a different behavior before arriving to the Z^{-2} time scale whose solutions have been obtained. In the latter case, a balance between inertial forces, instead of viscous ones, and surface tension shall be the correct one.

Chapter 3

Numerical simulations

In this chapter, we deal with the numerical simulations we have performed for the problem of the free-surface bounded retracting sheet of fluid. The simulations were done with the *Gerris* flow solver. We give a concise overview of the numerical and computational methods used by this solver.

3.1 The *Gerris* flow solver

The *Gerris* flow solver was developed by Stéphane Popinet and supported by the NIWA[1] and by the Marsden Fund of the RSNZ[2]. It is an open source free software written in C and uses object-oriented programming and the GLib and GTS libraries for the geometrical functions.

Spatial discretization

The spatial domain is discretized in squares organized hierarchically as a quadtree. This means that each cell may be the parent of four children cells. The level of a cell is defined as the number of ascendants it has as it is shown in Fig. 3.1.

The quadtree representation has been used as it has enormous advantages when dealing with the access of the data, *e.g.* efficient access to neighboring cells, cell level and spatial coordinates and efficient traversal of the leaf cells, same level cells and mixed cells.

Temporal discretization

The temporal discretization follows the classical fractional step projection method. At any given time n, the velocity field $\mathbf{U}^n$ and the fractional step pressure $p^{n-1/2}$

---

[1]National Institute of Water and Atmospheric research
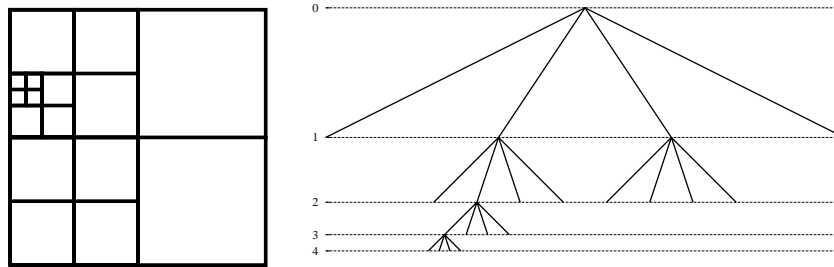[2]Royal Society of New Zealand

Figure 3.1: Quadtree representation. When the refinement is done, four children cells are created from a parent cell. The access to the data is the main advantage of using a quad tree structure.

are known at each cell center. Then a provisional value for the velocity $\mathbf{U}^*$ can be calculated integrating the Navier-Stokes equation in time assuming that the pressure is zero. The velocity field $\mathbf{U}^n$ and the pressure $p^{n+1/2}$ then may be computed by enforcing the incompressibility condition. This leads to the Poisson equation solving problem. The Poisson equation is discretized following then a linear problem that is solved through iterative methods using a relaxation operator.

Adaptive mesh refinement

When a tree-based structure is used, the refinement is not hard. The strategy that *Gerris* uses consists in two steps. First, any cell that satisfies a given criterion is refined bearing new children cells. In the second step, all the parent cells are checked. If any of them does not satisfy the refinement criterion, its children are killed and then the grid is coarsened.

The preset refinement criterion that *Gerris* uses is based on the vorticity field. If a cell matches, $\frac{h||\mathbf{U}||}{\max ||\mathbf{U}||} > \theta_{\mathrm{thr}}$, the cell is refined. We can depict the threshold θ_{thr} as the maximum angular deflection of a fluid particle that crosses a cell at a speed equal to the maximum over the whole domain.

Volume of fluid method

There are several ways of representing an interface in computational fluid dynamics. The numerical methods to achieve this can be explicit or implicit. In the former case, the interface is advected using a separate mesh for it that should be deformed and refined during the whole motion. In the latter, we use a fixed grid and a phase function that indicates in which phase we are at a given location. The interface can be constructed in terms of the zones of rapid variation of the
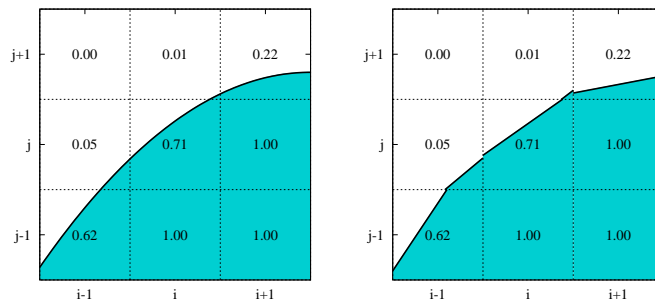
Figure 3.2: In the PLIC method, the interface is reconstructed with a piecewise linear function. Even a matching in the faces of the cell is not guaranteed, the discontinuities are very small.

phase function. The phase function can be advected with the fluid particles and the motion of the interface is then implicitly found.

The Volume Of Fluid or VOF technique is an implicit method that works with a discrete version of the phase function named color function. In the whole fluid, the color function has a monotone value (either one or zero) except in the cells crossed by the interface where the color function has a fractional value.

There are several methods for reconstructing the interface from this data. In the PLIC[3] method, the local shape of the interface is constructed with the discretized gradient of the color function and the volume fraction itself. This construction method does not satisfy the continuity of the interface in the face cells but the discontinuity is usually of order $\mathcal{O}(h^2)$ (see Fig. 3.2).

The second step of the VOF method deals with the advection of the interface. Once the shape of the interface is known, it is necessary to compute the amount of fluid exchanged between neighboring cells.

3.2 Specific numerical procedure details

This section is addressed to the details of the specific problem of the retracting fluid sheet.

We have chosen a rectangular spatial domain consisting of 3x1. The initial refinement level is 9. This means an initial mesh of 1536x512 points. For conserving resolution in the interface, another refinement criterion has been added to the typical vorticity refinement algorithm: when the phase has a value bigger than zero and smaller than one, the surround is refined. This assures a good resolution in the cells crossed by the interface.

The boundary and the initial conditions in the domain have been fixed as follows. The sheet occupies the bottom region taking advantage of the y-symmetry.

---

[3]Piecewise Linear Interface Calculation

The initial sheet consists of a planar sheet with circular tip with radius equal to the half of the sheet thickness. In the left boundary of the domain Neumann boundary conditions are imposed to the velocity field and Dirichlet's for the pressure. In the right boundary, Dirichlet's for the velocity field and Neumann condition for the pressure. Imposing a fluid incoming at the right is equivalent to place ourselves in a reference frame that moves with the speed at which the fluid enters. Choosing adequately this speed equal to the Taylor-Culick velocity is quite helpful as our sheet would remain inside our simulation domain.

A passive gas surrounds the sheet. We have chosen a density ratio of 0.1. The viscosity of the gas has been fixed at 0.0001 while the inner fluid viscosity has taken several values. This has been our parameter to variate as we have left the surface-tension and the density both constant and equal to one in all the simulations.

The numerical simulations have been performed for four different Ohnesorge's numbers of order 10^{-3}, 10^{-2}, 10^{-1} and 1. As we were interested in large timescale behavior, simulations took several hours and even days.

3.3 Results and discussion

The numerical results obtained by *Gerris* are shown in Figures 3.3 and 3.4 for a set of four Ohnesorge's number. They show the typical behavior expected: a growing rim that recedes with a speed that tends to the Taylor-Culick velocity. In fact, in our reference frame the rims tend to stay at rest as time grows. The first two cases may confirm us this as we have reached long enough times to see a *stationary* rim.

3.3.1 Neck formation and breakup

It is quite important to know for which Ohnesorge's values we have necks. These are regions where the thickness of the sheet has reduced by a purely hydrodynamical effect. Song and Trygvasson in 1998[7] observed that a neck was formed when the Ohnesorge's number was smaller than $Z \simeq 0.35$,[4]. This is very near with what we found in section 2.1.2 as critical value for neck formation $Z \simeq 1/2$. In our simulations we tried with an Ohnesorge number between our prediction and the observation of Song et al. and we didn't have neck. However, it is very risky to get any conclusion from the numerical simulations near the critical point because the neck may be damped by the code or even become unresolvable to the grid. On the other hand, our theoretical procedure has its own limitations because the long-wave limit hypothesis is weakened as we approach the rim.

What happens when the Ohnesorge number is lowered? Effectively, tighter necks are formed but this should be treated with care. In section 2.1.3 we found

---

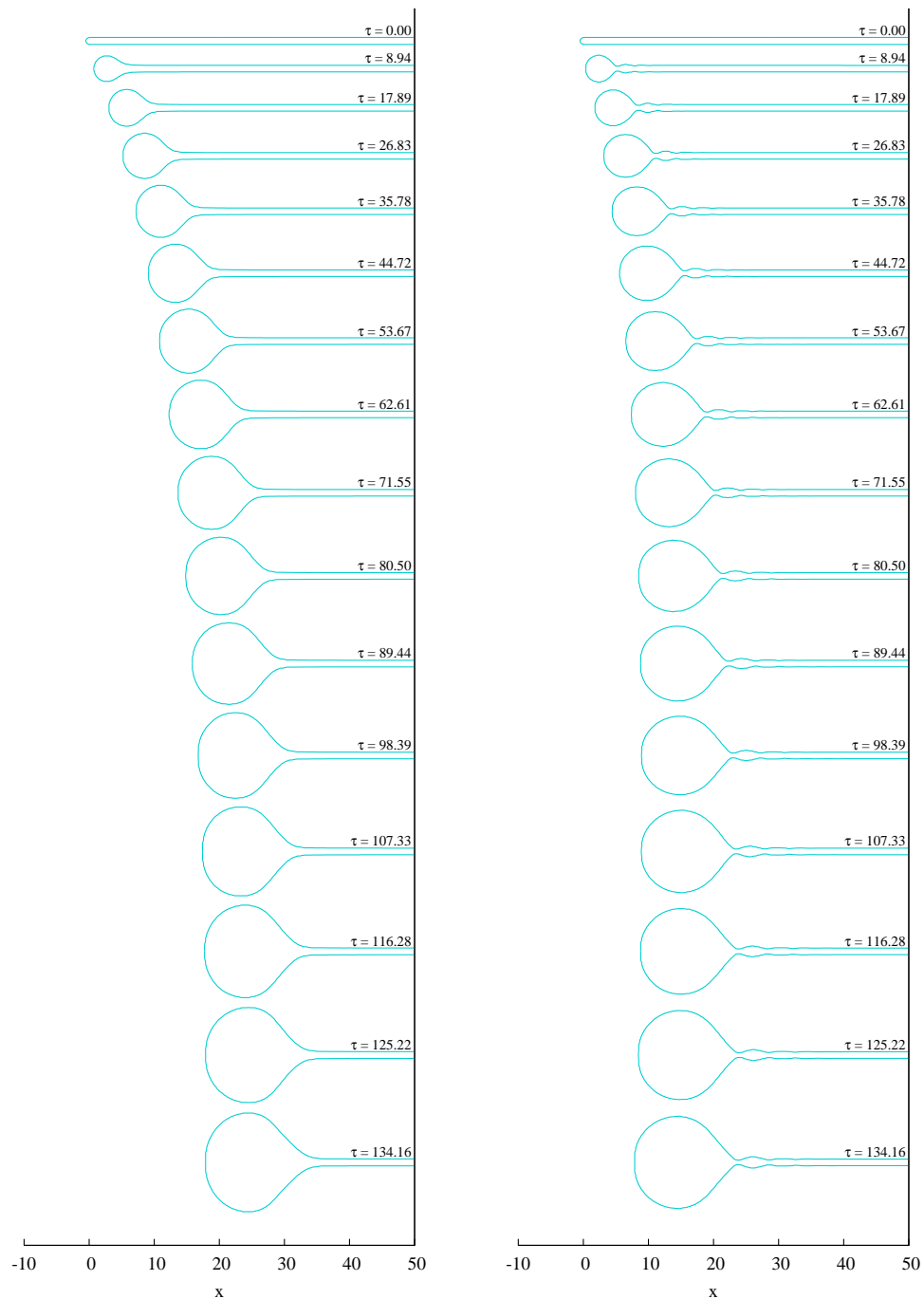[4]In fact, Song et al. found 0.25 but they defined the Ohnesorge number as $Z/\sqrt{2}$

Figure 3.3: Numerical simulations for $Z = 0.45$ and $Z = 0.045$. In both cases a drop-like structure develops at the edge of the fluid. In the former case the function decays monotonically towards the unperturbed far regions, while in the latter, small oscillations are present and a neck is formed.
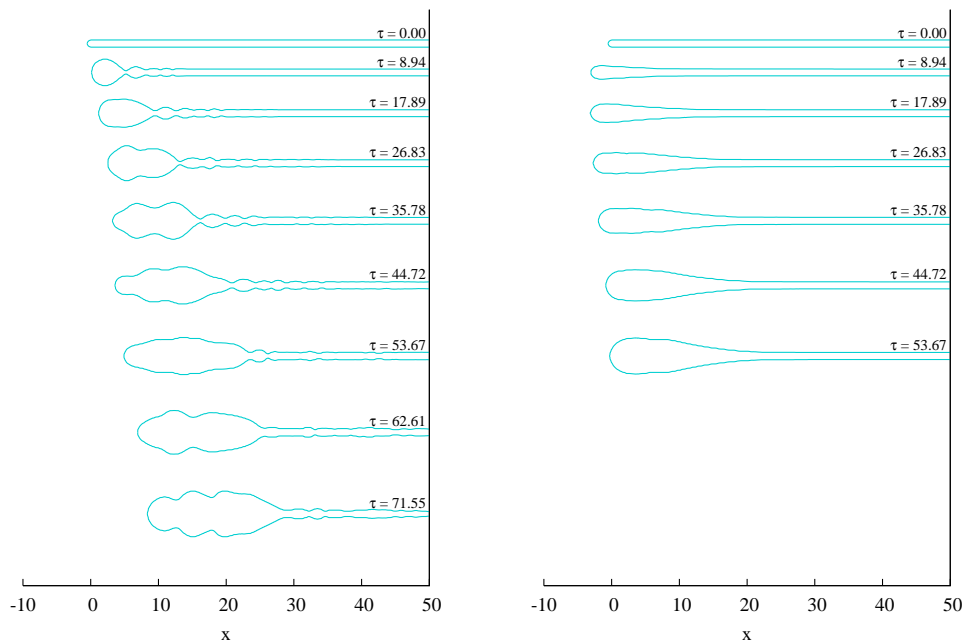
Figure 3.4: Numerical simulations for Z = 0.0045 and Z = 4.5. The situation changes dramatically in the two cases. In the first one, a neck is formed but subsequently the rim becomes unstable and turbulent. In the second one, the evolution is extremely slow due to high viscosity.

that the parabolic envelopes of the travelling wave solutions were controlled by the Ohnesorge number. As this is lowered, the slopes become more important and the long-wave limit hypothesis is broken for very small Ohnesorge's numbers. Moreover, there are more and more oscillations before reaching a uniform decay region. These may become very steep breaking also the long-wave limit hypothesis to the *right* of neck. The numerical simulations show that at the lowest Ohnesorge's number, a very tight neck is formed at the earlier stages but then a turbulent behavior dominates. As this occurs very rapidly, the constant speed hypothesis that we have used in section 2.1 fails and acceleration may become important.

Is it possible to have breakup by purely hydrodynamical effects in a fluid sheet as in the case of axisymmetrical jets? This cannot happen in 2-D fluid sheets. The self-similar solutions in the axisymmetric jets are possible because of the axial component of the curvature. Since this term does not exist in 2-D fluid sheets, the behavior is quite different and the neck does not shrink to zero as time passes and it converges quickly to a finite value. Song et al. suggested that the breakup may be reached in the low Ohnesorge number limit. Their prediction seems to be quite ambitious as we will have to deal with a complete turbulent

problem far from the transition.

3.3.2 Several timescales

The studied problem is quite complicated as it seems to have different timescales in the evolution of the shape of the sheet as it recedes. Figure 3.3 shows that probably three timescales exist in the problem. The first one is very short and deals with the transition from the initial condition to a earlier type of self-similar-like solution for the rim. This transition timescale seems to depend on Ohnesorge's number as viscosity opposes to rapid changes in the shape of the sheet.

Most of the stages plotted at Figure 3.3 are related with the second timescale. This stage shall be already independent of the initial condition[5]. The pear-shape of the self-similar-like rim in this stage is well defined. The rim is not circular at all. It consists of a circular part but also of a straight line near the joint which slope seems to be very close to $\sqrt{2}$ at least for the two Ohnesorge's values shown in Fig. 3.3 showing that it depends weakly on the parameter. This gives us the hint that at this timescale, some kind of balance independent of viscosity dominates. The candidates are inertia and surface tension for achieving this. It is also remarkable that during this stage the neck accelerates in contrast with the final timescale.

The last stage of evolution consists of a neck that asymptotically does not move and a growing rim that effectively tends to a circle. The *Gerris* numerical simulation for $Z = 0.045$ has just started to show this behavior at the final two plots in Fig. 3.3. In effect, it can be seen that the neck has stabilized and now the tip of the rim has started its motion to the opposite direction as consequence of the growth of the rim.

Even we have not been able to see a rim that tends to a circle in our numerical simulations because they took so long that we would have need some weeks for achieving it, the results of Sünderhauf, Raszillier and Durst[8] shows that this timescale does exist. They were able to reach non-dimensional times τ of order 10^3 where this stage is already well developed for $Z \sim 1$. Their results seem to be very similar to our theoretical results obtained in section 2.4. It would be very interesting to see if this stage can be reached for other Ohnesorge values. However this can be a very hard task as the timescale at which the stage is reached grows dramatically (see the discussion in section 2.4). Even though, the lower limit, as we have already seen, becomes turbulent so circular rims would not be seen at all.

---

[5]Just the y-symmetry should be preserved.

Conclusions

We have studied the time-dependent problem of an initially stationary 2-D fluid sheet that retracts by surface tension. The fluid was assumed to be viscous and incompressible and the boundaries were assumed to be free surfaces with constant surface tension.

The evolution of the shape of the sheet is characterized by a rim that accumulates mass as it retracts. The rim recedes with a speed that tends to a constant called the Taylor-Culick velocity. This speed can be found by momentum and mass conservation equations for the rim.

The fluid motion is governed by the Navier-Stokes equation. The solutions should be symmetrical in the y-axis. The whole problem is controlled by one dimensionless parameter called Ohnesorge's number, which is a quotient between viscous and surface tension forces.

In order to approach us to the solution, we have studied the behavior of waves in an infinite uniform fluid sheet. Considering just varicose modes, we have obtained a dispersion relation for them. All the modes are damped. However, it has been interesting to see that just some waves propagate. This is controlled by the Ohnesorge number. In the long wavelength limit, this occurs if the Ohnesorge number is smaller than $1/2$. Moreover, we have determined numerically that if the Ohnesorge number is bigger than 0.716, the propagation does not exist at all.

As an attempt to simplify the Navier-Stokes equations, we have used lubrication equations. These are an asymptotic limit of the Navier-Stokes equations for long-wave perturbations. The problem then was reduced to set of two coupled nonlinear equation that describes the motion of the sheet in terms of its thickness and horizontal speed.

Using the lubrication equations adding a correction to the curvature to avoid problems with the derivative divergency in the tip, we were able to find a whole domain asymptotical solutions for long times by studying three different regions in the sheet. The first region, far from the rim, behaves as stationary in a reference

frame that translates with the Taylor-Culick velocity. We have shown that the region may present oscillations: if $Z > 1/2$, the thickness of the sheet decays monotonically, else oscillations are present.

As the rim accumulates mass, the length scales are lost and self-similar solutions seem to well describe its behavior. Making an asymptotic expansion in time of lubrication equations we have found circular solutions in the first order.

In order to match the self-similar rim with the stationary region far from the rim, we had to look for an intermediate region. This region is also self-similar but with different self-similar variables than the rim. Once this region was found, we were able to construct a whole domain solution. When constructing it, very strong constraints for the timescales have appeared for low as for high Ohnesorge's numbers.

We have also performed numerical simulations of the complete Navier-Stokes equations to verify our results. The simulations were done using *Gerris*, a code whose special characteristic is the usage of quadtree data structures. The interfaces were treated with the volume of fluid technique. The code was run for a wide range of Ohnesorge's numbers, 10^{-3} to 10.

The numerical simulations agree with the predictions. The rims recede with the asymptotically Taylor-Culick velocity. The Ohnesorge number controls the rate at which this velocity is reached. It is quite remarkable also that when the Ohnesorge number is lowered too much, turbulent behavior is observed in the sheet.

Necks are formed if the Ohnesorge number is below a critical value. Even we have not been able to measure this critical value to compare it with our theoretical prediction, we had the observation made by Song et al., that this occurs at $Z \simeq 0.35$. The result is quite near our prediction and it is likely underestimated due to numerical simulations restrictions. The formation of a neck by purely hydrodynamic effect and a possible breakup has been discussed.

The numerical simulations show that three timescales can be well observed in the evolution of the shape of the sheet. The first one deals with the transition from the initial condition to the second one, which is governed by a growing self-similar rim but with an important acceleration still present at the neck. The final stage, by contrast shows a stationary neck with a self-similar rim that tends effectively to a circle. Our code was able to run fine within the first two stages but the simulations take much so long that we were able to reach it hardly. Our theoretical results were focused justly to the largest timescale, and we had not enough data to make the comparison. However, using the results of Sünderhauf et al., we were able to confirm that this timescale does exist and that our whole domain solutions seem to quite fit their numerical solution at least for $Z = 1$.

Bibliography

[1] M. P. Brenner and D. Gueyffier. On the bursting of viscous films. *Physics of Fluids*, 11:737–739, March 1999.

[2] J. Eggers and T. F. Dupont. Drop formation in a one-dimensional approximation of the Navier-Stokes equation. *Journal of Fluid Mechanics*, 262:205–221, 1994.

[3] T. Erneux and S. H. Davis. Nonlinear rupture of free films. *Physics of Fluids*, 5:1117–1122, May 1993.

[4] H. Lamb. *Hydrodynamics*. Cambridge University Press, Cambridge, U.K., 6th edition, 1932.

[5] A. Oron, S. H. Davis, and S. G. Bankoff. Long-scale evolution of thin liquid films. *Reviews of Modern Physics*, 69:931–980, July 1997.

[6] S. Popinet. Gerris: a tree-based adaptive solver for the incompressible Euler equations in complex geometries. *Journal of Computational Physics*, 190:572–600, September 2003.

[7] M. Song and G. Tryggvason. The formation of thick borders on an initially stationary fluid sheet. *Physics of Fluids*, 11:2487–2493, September 1999.

[8] G. Sünderhauf, H. Raszillier, and F. Durst. The retraction of the edge of a planar liquid sheet. *Physics of Fluids*, 14:198–208, January 2002.

[9] G. Taylor. The dynamics of thin sheets of fluid. III. Disintegration of fluid sheets. *Royal Society of London Proceedings Series A*, 253:313–321, December 1959.

[10] G. Tryggvason, R. Scardovelli, and S. Zaleski. *Computational methods for drops, bubbles and interfaces*. Cambridge University Press (to appear), Cambridge, U.K., 2008.